

Results from the first all-sky search for continuous gravitational waves from small-ellipticity sources

Vladimir Dergachev^{1,2, a} and Maria Alessandra Papa^{1,2,3, b}

¹*Max Planck Institute for Gravitational Physics (Albert Einstein Institute), Callinstrasse 38, 30167 Hannover, Germany*

²*Leibniz Universität Hannover, D-30167 Hannover, Germany*

³*University of Wisconsin Milwaukee, 3135 N Maryland Ave, Milwaukee, WI 53211, USA*

We present the results of an all-sky search for continuous gravitational wave signals with frequencies in the 500-1700 Hz range targeting neutron stars with ellipticity of 10^{-8} . The search is done on LIGO O2 data using the Falcon analysis pipeline. The results presented here double the sensitivity over any other result on the same data [12, 31]. The search is capable of detecting low ellipticity sources up to 170 pc. We establish strict upper limits which hold for worst-case signal parameters. We list outliers uncovered by the search, including several which we cannot associate with any known instrumental cause.

Introduction Continuous gravitational waves are expected over a broad range of frequencies from rapidly rotating compact stars such as neutron stars due to a variety of mechanisms [1], as well as from more exotic scenarios [2–7].

A spinning neutron star that presents a deviation from axi-symmetry emits continuous gravitational waves at twice its rotation frequency. Its gravitational-wave brightness is determined by its equatorial ellipticity, which describes how deformed the star is in the plane perpendicular to the rotation axis. Because neutron stars have solar sized mass packed within a tight radius of 10-15 km, the gravity at their surface is extremely high, making it difficult to support large deformations.

Simulations show that ellipticities as high as 10^{-6} can be supported by the crust [8, 9], but at present no mechanism is known that mandates the existence of such deformations. Searches so far have failed to find signals from high ellipticity sources [10–14].

On the other hand, properties of observed pulsars suggest that a population might exist whose spin evolution is governed by gravitational wave emission, with typical ellipticities in the range of $\approx 10^{-9}$ to 10^{-8} [15]. This is the range targeted by this search (Figure 1).

We find several outliers and investigate them. We use longer coherence analyses and out-of-sample data. One outlier increases in SNR with increase in coherence length, however, this increase is not as large as one would expect for an ideal signal on average.

The basic signal assumed at the gravitational wave detector is a nearly monochromatic signal from an isolated source (i.e. not in a binary), with Doppler modulations due to the relative motion between the source and the detector and amplitude modulations due to the relative orientation of the detector to the source. Optimal sensitivity is typically achieved with a large degree of phase coherence in the signal and for signals matching the assumed waveform model.

No past search has revealed any such signal, over a broad range of possible signal parameters. One reason

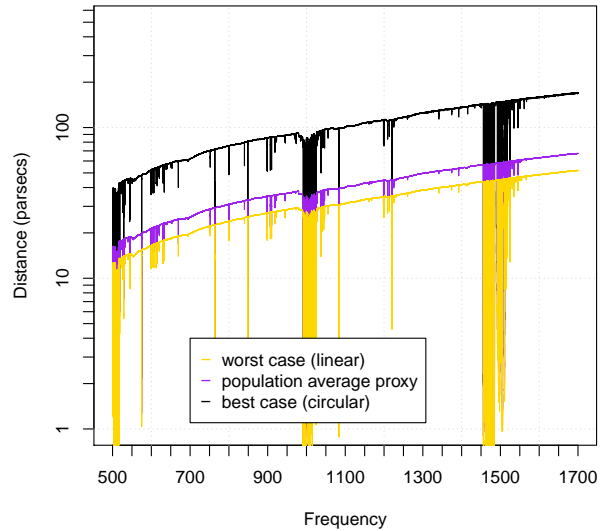


FIG. 1. Range of the search for stars with ellipticity of 10^{-8} . The X axis shows gravitational wave frequency, which is twice the pulsar rotation frequency for emission due to an equatorial ellipticity. R-modes and other emission mechanisms give rise to emission at different frequencies.

could be that past searches were not sensitive enough and have not yet probed low enough values of the ellipticity. Another reason (or perhaps an additional reason) might be that the signals deviate enough from the assumed model that the search methods cannot identify them with sufficient confidence.

Deviations from the naive signal model could come about in a number of ways, for example due to the motion of the source being affected by another body, or the signal itself not being perfectly stable. While standard searches might retain very good sensitivity to many of these signals [16], upon closer inspection a signal candidate might be disregarded because it does not pass all

the tests that the naive signal would pass.

As more and more sensitive searches yield null results it seems wise to entertain the possibility that the signals are not quite as we assume. Here we do this by highlighting not only the upper limit results for the standard signals, but also the top outliers that are marginal/inconclusive candidates. This will enable cross-checks with data that we have no access to, and may lead to the identification of an instrumental or environmental artefact, or a signal.

The method Broad-band all-sky searches for continuous gravitational waves are computationally challenging. The most sensitive surveys employ multi-stage searches that rely on clever search methods, computationally efficient algorithms and much computing power.

A key characteristic of long-duration searches is the employed coherence length. Increasing the coherence length increases the search sensitivity and makes the search more selective, being able to distinguish more finely different signal parameters like sky location and frequency. The number of separate points of parameter space that need to be explored grows with the increasing coherence length and this generates greater computational demands. The computational cost can scale as the fourth power of the coherence length for even simple searches and it grows very quickly for searches taking into account more complex signals, with higher order frequency derivatives or in the presence of a companion object in a binary system.

A common way to construct a search with a given coherence length is to partition the data into segments spanning that coherence length, perform a matched filter analysis on each piece and then combine the results. This is known as a “semi-coherent” search, because the results of the coherent matched filter analysis are combined with no phase information. See [13, 14, 17–19] and references therein for an overview and comparison of the different families of semi-coherent search methods.

Loosely coherent methods [20–22] are constructed by partitioning the parameter space of the searched signals into families of closely related signals that can be considered to be perturbations of each other. The search is then designed to work on each family separately and because many signals are searched for “at the same time” it leverages significant economy of scale.

The newest loosely coherent implementation targeting longer coherent timescales, the Falcon search, represents a breakthrough in performance and sensitivity [13]. We have explored the LIGO O1-run data employing the Falcon search with a first-stage coherence length of 4 hours, and demonstrated its performance and computational efficiency [10, 13]. In this paper we push the envelope further, doubling the size of the input data, tripling the coherence length of the first stage, extending the frequency range by a factor of nearly three and searching high fre-

quencies¹. We attain more than a two-fold increase in strain sensitivity with respect to the best LIGO all-sky search on the same data (Figure 2).

The search The computational load of an all-sky search per-Hz-searched is massively different in the kHz region and in the $O(100)$ Hz region. This means that in order to achieve optimal sensitivity different search set-ups should be used in different frequency ranges (this argument is clearly illustrated in [23, 24]). We choose here to tackle the challenging high-frequency region. We aim at detecting continuous gravitational wave signals with frequency between 500 – 1700 Hz and first-order frequency derivative $|f_1| \leq 3 \times 10^{-12}$ Hz/s for frequencies below 1000 Hz and $\leq 2.5 \times 10^{-12}$ Hz/s above 1000 Hz. The spindown range is consistent with our ellipticity target at a level $< 10^{-8}$. It is also generous: the largest known frequency drift among pulsars spinning faster than 250 Hz is -1.73×10^{-13} Hz/s, for J1824-2452A spinning at 327 Hz [25]. The full search parameter range is given in Table II.

We use the public LIGO [26] O2 data [27, 28]. Below 1000 Hz this data was subject to a cleaning procedure that removed a substantial amount of spurious instrumental noise [29]. In general this procedure will contribute an additional systematic uncertainty to the calibration, which is however not stated. We use the available O2 data as is, thus our results below 1000 Hz have a potential systematic uncertainty that overall should match the uncertainty (5% and 10% for H1 and L1 respectively) given in LIGO papers such as [12].

The search begins with a coherence length of 12 hours that is extended to 6 days through 3 follow-up stages (Table I). The coherence length increases from stage to stage and with it the search sensitivity also increases. Candidates pass to the next stage only if their detection statistic value exceeds a predetermined threshold value, which increases from one stage to the next. The last stage also includes consistency checks between the single-instrument results. Candidates that survive this entire sequence of tests represent one of the results of the search. We refer to these as the *outliers* from the search. Every outlier is defined by a set of signal parameters (frequency, sky position and frequency derivative) and signal to noise ratio value (SNR).

¹ The necessary computing power scales as the cube of highest frequency searched

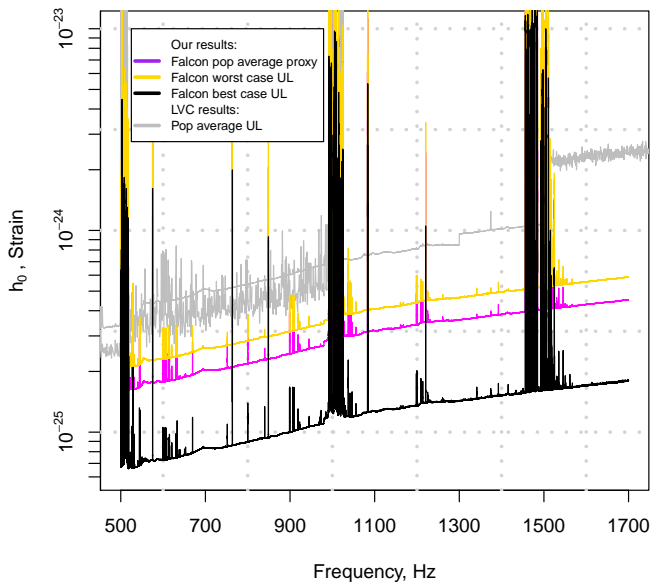


FIG. 2. The intrinsic gravitational-wave strain-amplitude upper-limit (vertical axis) is plotted against signal frequency. The lower curve (black) shows the best-case upper limits (circularly polarized signals), the next curve (purple) shows the population-average proxy, then (in yellow) we have the worst-case upper limits. The fainter lines at the top are the upper limits from the latest LIGO-Virgo collaboration (LVC) all-sky survey [12] and they can be directly compared to our population-average ones (middle purple curve). The LVC results are produced independently by three different pipelines which cover overlapping frequency ranges.

Stage	Coherence length (hours)	Minimum SNR
0	12	6
1	24	7
2	48	8
3	144	16

TABLE I. Parameters for each stage of the search. The stage 3 outliers are subject to an additional consistency check.

Band [Hz]	$ f_1 _{\max}$ 10^{-12} [Hz/s]	$ f_2 _{\max}$ 10^{-20} [Hz/s ²]
500-1000	3	4
1000-1700	2.5	2

TABLE II. Signal-parameter space covered in this search. Both positive and negative values of first and second order frequency derivatives f_1 and f_2 are explored.

Upper limit results The other results of this pa-

per are the 95% confidence-level continuous gravitational wave amplitude upper limits h_0 . These represent the smallest amplitude of a continuous signal with a given frequency, coming from an arbitrary direction in the sky and with frequency drift in our search range, that we can exclude from impinging on the detectors. We have assumed a quasi-monochromatic signal with slow evolution in frequency that can be approximated by a quadratic model:

$$f(t) = f_0 + (t - t_0)f_1 + (t - t_0)^2 f_2/2, \quad (1)$$

where f_0 is the signal frequency at GPS epoch $t_0 = 1183375935$, and f_1 and f_2 are the linear and quadratic frequency drifts, respectively.

Our upper limits are established based on the observed power estimates and are valid even in the most heavily contaminated spectral regions. We use a procedure based on the so-called “universal statistics” [30] which determines the smallest gravitational wave intrinsic signal amplitude h_0 consistent with the observed power. This produces valid upper limits without assumptions on the shape of the noise distribution. By construction the upper limits also hold in the presence of a signal.

We compute three upper-limits: the so-called worst-case upper limit which is the largest upper limit over those established for individual sky locations, polarization², spindown and frequency; the circular-polarization upper limit which is the largest upper limit over those established for individual sky locations, spindown and frequency, having assumed circular polarization of the signal; and finally a proxy for the population-average upper limit which is determined over a population of sources uniformly distributed on the sky and with all possible polarizations (uniform in the cosine of the inclination angle ($\cos \iota$) and polarization angle ψ). This last upper limit is provided for ease of comparison with other search results [11, 14, 31, 32] and it is estimated (hence it is a proxy) as a weighted average of the upper limits from the individual polarizations.

The population average proxy is verified by directly measuring the detection efficiency of fake signals added to the real data with frequencies in the sample bands 500-600 Hz and 1075.40-1100 Hz band. Each fake signal has an intrinsic strain amplitude h_0 equal to the population-average upper-limit proxy value from its frequency band; other parameters are uniformly distributed in the searched parameter space, apart for the spindown values that are log-uniformly distributed in the search range. The full analysis is performed for each fake signal, covering the entire sky and including outlier follow-up. A fake signal is considered detected when an outlier is

² maximum over polarization is usually reached for linear polarizations

found within 5×10^{-5} Hz of the signal frequency f , within 10^{-12} Hz/s of its spindown, and within $0.06 \text{ Hz}/f$ radians of its sky location, the latter calculated after projecting on the ecliptic plane (“ecliptic distance”). We obtain 95% recovery of injections everywhere except the heavily contaminated violin mode region, and even in those bands the detection efficiency does not drop lower than 90%.

The upper limits are plotted in Figure 2. The upper limit data is available in computer-readable format at [33].

Assuming an optimally oriented source of ellipticity 10^{-8} we are sensitive as far as 170 pc at 1700 Hz. Figure 1 shows the reach of the search to such sources. Above 700 Hz, with the exception of a few contaminated frequency bands, we can exclude the presence of such sources (aside from the outliers listed in Table III) within a 20 pc distance from Earth.

It is reasonable to expect neutron stars from our target population within this range: assuming a galactic population of 10^9 neutron stars, if the density in space of neutron stars is the same as that of the known pulsars, then within 20 pc of Earth we expect³ to have as many neutron stars and we observe as pulsars in ~ 1.36 kpc. At the time of writing the ATNF catalog shows 56 pulsars rotating above 250 Hz within 1.36 kpc of Earth and of these 12 are isolated.

Our upper limits are also relevant for boson condensates around black holes [3, 4], which are expected to emit monochromatic continuous wave signals [34]. Indeed, if ultralight bosons exist, they will form clouds around rotating black holes via superradiance instability and through annihilations and level transitions will emit continuous gravitational waves. We leave it to the interested reader to constrain from our upper limits physical quantities of interest, based on the specific model they wish to consider. Assuming the ensemble signal of [35] from a galactic population of $O(10^8)$ isolated stellar mass black holes with maximum mass $30 M_\odot$ and maximum initial spin uniformly distributed in $[0,1]$, our results exclude bosons with masses in the range $\approx [1.0-3.0] \times 10^{-12}$ eV.

Outliers The full list of outliers is available in [33]. Table III shows a summary of this list produced by displaying the largest SNR outlier in every 0.1 Hz band. This is especially helpful for the loud fake signals present in the data stream for validation purposes [36], since these produce many outliers. Because these fake signals are produced directly at the LIGO detectors by an appropriate excitation of its mirrors, they are commonly referred

to as “hardware injections”. In Table IV for convenience we give the parameters of these fake signals.

Our top 8 outliers in Table III are caused by such hardware-injections. The large majority of the remaining outliers are due to large hardware artifacts, as indicated in the last column of III. There remain outliers whose origin could perhaps be identified based on data from physical and environmental monitoring channels. Since this data is not public we cannot perform such investigations.

A key question is whether any of the listed outliers are produced by an astrophysical source. The simulations performed to verify the population average proxy assure us that if a signal were present in the data with detectable strength, there would be a corresponding outlier in Table III. Clearly none of the outliers due to hardware injections are astrophysical. A number of outliers are not due to hardware injected signals but are located in frequency bands with instrumental contamination. As the pipeline is perfectly able to detect signals in most heavily contaminated bands this does not rule out these outliers. However, it does cast doubt on their significance as contamination can artificially increase the SNR in a single or both instruments.

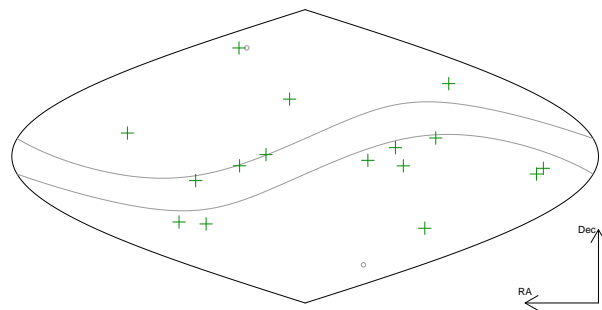


FIG. 3. Location in the sky of the outliers not associated to any instrumental disturbance. The wide band shows the ecliptic plane, the two small circles are the ecliptic poles.

The 16 outliers not associated with any known instrumental disturbance are the most interesting. Their sky locations are shown in Figure 3. They do not appear to cluster in any location tied to instrumental artifacts, such as the ecliptic pole. If the outliers were due to astrophysical signals that follow the frequency model of Eq. 1, then the uncertainty on their true location would be within the limits established by the Monte Carlo simulations discussed above, i.e. $0.06 \text{ Hz}/f$ radians, projected on the ecliptic plane.

The frequency spectrum of the data around these outliers is manually examined and none reveals any obvious contamination. As an example we show plots (Figures 4 and 5) corresponding to the highest-frequency outlier 43 at 1224.75 Hz. The apparent frequency of a signal with the parameters of outlier 43, spans almost 0.25 Hz dur-

³ This conservative estimate assumes spherical distribution of neutron stars. Since 1.36 kpc is large compared to the thickness of Milky Way disk and size of galactic arms, we expect that the true number is much larger.

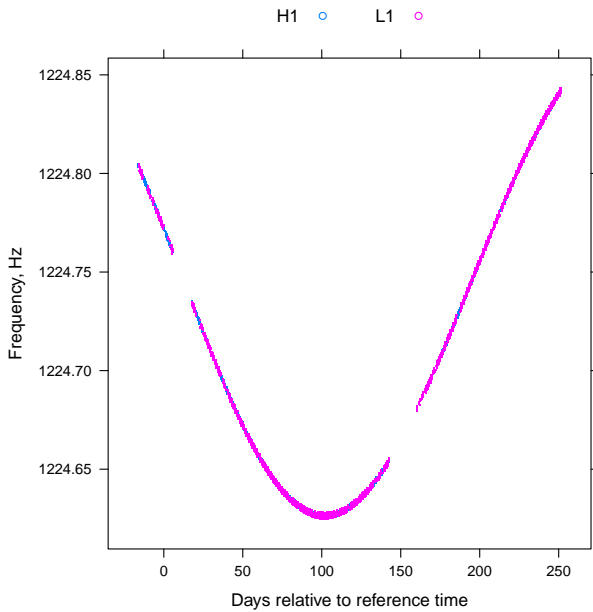


FIG. 4. Apparent frequency of a signal with parameters equal to those of outlier 43 at 1224.74 Hz, at the detectors. The difference in Doppler shifts between interferometers is small compared to the Doppler shifts from the Earth’s orbital motion.

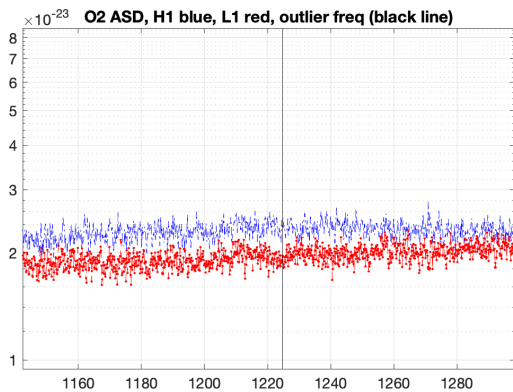


FIG. 5. Average amplitude spectral density around the frequency of outlier 43.

ing the O2 observing time and its evolution is shown in Figure 4.

The other 15 outliers have similar characteristics. The frequency evolution curves change depending on the outlier parameters but they all exhibit an appreciable modulation.

Ad-hoc investigations are focused on outliers 25 and 43, which are consistently found with both the Falcon and semi-coherent F-statistic analyses. Follow-ups over longer coherence lengths (up to 500 hours) suggest that the most promising outlier is outlier 25. We note that the f_1 value of outlier 25 is positive which would mean

that, if the outlier were associated to an astrophysical continuous signal, what is observed is *not* directly related to the spin frequency of the star.

The SNR build-up for outlier 25 over searches with increasingly long coherent time baseline is not inconsistent with what is expected from a signal. This holds true also for the fully coherent search over the O2 data, albeit the recovered SNR is lower than the expectation value based on the previous stages and with indications that the coherence might not be completely stable⁴. A follow-up on O1 data is inconclusive: the detection statistic value is not inconsistent with the expectations under the signal hypothesis, and the Gaussian-noise p-value is $\lesssim 1\%$.

As already pointed out, we are unable to investigate the O1 and O2 instrumental data channels, as this data is not part of either the O1 or O2 public data releases.

A first detection can be á-la GW150914 (the first gravitational wave signal [37]) with a single loud event that spectacularly meets all the predictions; a less glamorous scenario is that evidence builds up over time with outliers first identified in a broad survey like this and later consistently recovered on new data or through the identification of an electromagnetic counterpart. In this spirit we report and discuss the outliers that we find.

Our outliers are not present in the outlier or sub-threshold candidate lists from earlier papers. This is not surprising, because previous searches on LIGO O2 data that cover the parameter space of this search [12, 31] are significantly less sensitive.

The O3 data is roughly a factor of 2 more sensitive than the O2 data employed in this search so the LVC broadband searches should be able to probe continuous gravitational wave amplitudes comparable to these. Also, targeted searches based on the information presented here, which are comparatively less complex than these broad surveys, should be straightforward. We look forward to comparing our results on O3 data with those from the LVC, and we are ready to perform fast-turnaround investigations on new data.

ACKNOWLEDGEMENTS

The search was performed on the ATLAS cluster at AEI Hannover. We thank Bruce Allen, Carsten Aulbert and Henning Fehrmann for their support. We also acknowledge useful discussion with Bruce Allen on the distribution of nearby neutron stars.

This research has made use of data, software and/or web tools obtained from the LIGO Open Science Center

⁴ The most significant measured $2\mathcal{F}$ value is ≈ 47 . $2\mathcal{F}$ is the optimal multi-detector fully coherent detection statistic [38] for signals of the type of Eq. 1.

Idx	SNR	Frequency Hz	Spindown pHz/s	RA _{J2000} degrees	DEC _{J2000} degrees	Description
1	15792.0	763.84732	-0.20	198.894	75.690	Injected pulsar ip9
2	11970.1	575.16352	-0.20	215.256	3.445	Injected pulsar ip2
3	2470.1	848.95675	-0.80	38.563	-30.432	Induced by injected pulsar ip1
4	88.7	1220.55117	0.00	218.862	24.074	Injected pulsar ip7
5	64.1	575.20332	-1.80	184.911	38.083	Induced by injected pulsar ip2
6	38.1	849.00348	2.60	67.737	-11.166	Induced by injected pulsar ip1
7	36.3	848.89699	1.00	353.084	-56.879	Induced by injected pulsar ip1
8	26.4	763.77799	-2.20	222.633	-68.689	Induced by injected pulsar ip9
9	22.3	1004.27599	-1.08	294.094	-88.258	Disturbed H1 spectrum, lines in L1
10	19.8	986.28829	-3.20	21.424	75.556	Coincident lines in H1 and L1
11	19.4	1006.24309	1.08	97.733	-67.657	Disturbed H1 spectrum, lines in L1
12	18.4	575.09518	-2.00	296.704	30.014	Induced by injected pulsar ip2
13	18.2	990.50363	-3.60	318.140	61.085	Line in L1
14	18.1	1392.54524	-0.70	236.558	43.756	Induced by injected pulsar ip4
15	17.7	900.21880	-2.20	119.428	-5.859	
16	17.6	1021.84249	-0.70	13.986	-8.813	Sharp line in L1
17	17.6	968.58972	-1.80	338.891	-76.549	Line in H1
18	17.4	1392.47501	-0.72	215.544	-33.472	Induced by injected pulsar ip4
19	17.4	514.14893	1.60	124.356	5.300	
20	16.9	1220.62294	1.44	256.566	65.131	Induced by injected pulsar ip7
21	16.8	997.54586	-1.80	210.349	46.174	Disturbed H1 spectrum
22	16.8	995.20385	1.40	205.113	48.184	Disturbed H1 spectrum
23	16.7	1001.36623	4.30	77.684	-44.133	
24	16.6	676.19542	2.80	220.418	-5.822	
25	16.6	744.21917	2.40	191.654	35.097	
26	16.5	998.97311	-2.00	51.221	11.566	Disturbed H1 spectrum, line in L1
27	16.4	997.41470	1.40	345.963	-27.957	Disturbed H1 spectrum
28	16.4	991.29230	2.20	48.300	-60.960	Disturbed H1 spectrum
29	16.4	512.49081	1.20	141.462	-2.467	
30	16.3	991.10725	0.40	313.415	61.938	Disturbed H1 spectrum, line in L1
31	16.3	983.15189	2.20	204.037	1.030	
32	16.3	988.60680	1.80	145.053	-44.240	Lines in H1 and L1
33	16.3	510.79524	-2.40	23.196	-5.131	Disturbed L1 spectrum
34	16.2	886.88009	-1.60	281.482	-40.307	
35	16.2	988.37320	1.20	56.255	44.595	
36	16.2	512.26233	3.00	334.102	-12.737	Line in L1
37	16.2	963.34281	-2.80	306.751	59.163	Line in H1
38	16.2	1580.37607	-2.50	11.198	32.482	Line in L1
39	16.1	514.29168	3.20	32.603	-7.354	
40	16.1	831.98847	0.40	281.743	66.494	
41	16.1	873.52461	0.40	35.466	-10.855	
42	16.1	895.42195	3.60	292.529	14.276	
43	16.0	1224.74567	-2.16	98.278	11.241	
44	16.0	1014.34897	-2.50	25.330	82.271	Lines in H1 and L1
45	16.0	698.72803	-0.20	261.117	-41.490	
46	16.0	1095.55740	-1.08	249.504	-14.911	

TABLE III. Outliers produced by the detection pipeline. Only the highest-SNR outlier is shown for each 0.1 Hz frequency region. Outliers marked with “line” have strong narrowband disturbances near the outlier location. Signal frequencies refer to GPS epoch 1183375935.

(<https://losc.ligo.org>), a service of LIGO Laboratory, the LIGO Scientific Collaboration and the Virgo Collaboration. LIGO is funded by the U.S. National Science Foundation. Virgo is funded by the French Centre National de Recherche Scientifique (CNRS), the Italian Istituto Nazionale della Fisica Nucleare (INFN) and the Dutch Nikhef, with contributions by Polish and Hungar-

ian institutes.

Label	Frequency Hz	Spindown pHz/s	RA _{J2000} degrees	DEC _{J2000} degrees
ip1	848.969641	300	37.39385	-29.45246
ip2	575.163521	-0.137	215.25617	3.44399
ip4	1393.540559	-254	279.98768	-12.4666
ip7	1220.555270	-1120	223.42562	-20.45063
ip9	763.847316	-1.45×10^{-5}	198.88558	75.68959

TABLE IV. Parameters of the hardware-injected simulated continuous wave signals during the O2 data run (GPS epoch 1130529362).

^a vladimir.dergachev@aei.mpg.de

^b maria.alessandra.papa@aei.mpg.de

- [1] P. D. Lasky, Gravitational Waves from Neutron Stars: A Review, *Publ. Astron. Soc. Austral.* **32**, e034 (2015)
- [2] R. Brito, S. Ghosh, E. Barausse, E. Berti, V. Cardoso, I. Dvorkin, A. Klein and P. Pani, Gravitational wave searches for ultralight bosons with LIGO and LISA, *Phys. Rev. D* **96**, no. 6, 064050 (2017)
- [3] M. Baryakhtar, R. Lasenby, M. Teo, Black Hole Super-radiance Signatures of Ultralight Vectors, *Phys. Rev. D* **96**, 035006s (2017)
- [4] A. Arvanitaki, M. Baryakhtar, R. Lasenby, S. Dimopoulos, S. Dubovsky, Black Hole Mergers and the QCD Axion at Advanced LIGO, *Phys. Rev. D* **95**, 043001 (2017)
- [5] A. Arvanitaki, M. Baryakhtar, X. Huang, Discovering the QCD Axion with Black Holes and Gravitational Waves, *Phys. Rev. D* **91**, 084011 (2015)
- [6] C. J. Horowitz and S. Reddy, Gravitational Waves from Compact Dark Objects in Neutron Stars, *Phys. Rev. Lett.* **122**, no. 7, 071102 (2019)
- [7] C. J. Horowitz, M. A. Papa and S. Reddy, Gravitational waves from compact dark matter objects in the solar system, arXiv:1902.08273
- [8] C. J. Horowitz and K. Kadau, Breaking Strain of Neutron Star Crust and Gravitational Waves, *Phys. Rev. Lett.* **102**, 191102 (2009).
- [9] N. K. Johnson-McDaniel and B. J. Owen, Maximum elastic deformations of relativistic stars, *Phys. Rev. D* **88**, 044004 (2013)
- [10] V. Dergachev and M. A. Papa, Results from an extended Falcon all-sky survey for continuous gravitational waves, *Phys. Rev. D* **101**, 022001 (2020)
- [11] B. P. Abbott *et al.* (LIGO Scientific Collaboration and Virgo Collaboration), Full Band All-sky Search for Periodic Gravitational Waves in the O1 LIGO Data, *Phys. Rev. D* **97** 102003 (2018).
- [12] B. P. Abbott *et al.* (LIGO Scientific Collaboration and Virgo Collaboration), All-sky search for continuous gravitational waves from isolated neutron stars using Advanced LIGO O2 data, *Phys. Rev. D* **100** 024004 (2019).
- [13] V. Dergachev and M. A. Papa, Sensitivity Improvements in the Search for Periodic Gravitational Waves Using O1 LIGO Data, *Phys. Rev. Lett.* **123**, no. 10, 101101 (2019)
- [14] B. P. Abbott *et al.* (LIGO Scientific and Virgo Collaborations), First low-frequency Einstein@Home all-sky search for continuous gravitational waves in Advanced LIGO data, *Phys. Rev. D* **96**, no. 12, 122004 (2017)
- [15] G. Woan, M. D. Pitkin, B. Haskell, D. I. Jones, and P. D. Lasky, Evidence for a Minimum Ellipticity in Millisecond Pulsars, *ApJL* **863** L40 (2018)
- [16] A. Singh, M. A. Papa and V. Dergachev, Characterizing the sensitivity of isolated continuous gravitational wave searches to binary orbits, *Phys. Rev. D* **100** (2019) no.2, 024058 doi:10.1103/PhysRevD.100.024058
- [17] S. Walsh, K. Wette, M. A. Papa and R. Prix, Optimizing the choice of analysis method for all-sky searches for continuous gravitational waves with Einstein@Home, *Phys. Rev. D* **99**, no. 8, 082004 (2019)
- [18] S. Walsh *et al.*, Comparison of methods for the detection of gravitational waves from unknown neutron stars, *Phys. Rev. D* **94**, no. 12, 124010 (2016)
- [19] C. Dreissigacker, R. Prix, K. Wette, Fast and Accurate Sensitivity Estimation for Continuous-Gravitational-Wave Searches, *Phys. Rev. D* **98**, 084058 (2018)
- [20] V. Dergachev, On blind searches for noise dominated signals: a loosely coherent approach, *Class. Quantum Grav.* **27**, 205017 (2010).
- [21] V. Dergachev, Loosely coherent searches for sets of well-modeled signals, *Phys. Rev. D* **85**, 062003 (2012)
- [22] V. Dergachev, Loosely coherent searches for medium scale coherence lengths, *Phys. Rev. D* **85**, 062003 (2012)
- [23] J. Ming, B. Krishnan, M. A. Papa, C. Aulbert and H. Fehrmann, *Phys. Rev. D* **93** (2016) no.6, 064011 doi:10.1103/PhysRevD.93.064011
- [24] J. Ming, M. A. Papa, B. Krishnan, R. Prix, C. Beer, S. J. Zhu, H. B. Eggenstein, O. Bock and B. Machenschalk, *Phys. Rev. D* **97** (2018) no.2, 024051 doi:10.1103/PhysRevD.97.024051
- [25] R.N. Manchester, G.B. Hobbs, A. Teoh, M. Hobbs, *AJ*, 129, 1993-2006 (2005)
- [26] J. Aasi *et al.* (LIGO Scientific Collaboration), Advanced LIGO, *Class. Quantum Grav.* **32** 7 (2015)
- [27] M. Vallisneri *et al.* The LIGO Open Science Center, proceedings of the 10th LISA Symposium, University of Florida, Gainesville, 2015 *J. Phys.: Conf. Ser.* 610 012021
- [28] LIGO Open Science Center, <https://doi.org/10.7935/CA75-FM95>, (2019)
- [29] J.C. Driggers *et al.* (LIGO Scientific Collaboration Instrument Science Authors), Improving astrophysical parameter estimation via offline noise subtraction for Advanced LIGO, *Phys. Rev. D* **99**, 042001 (2019).
- [30] V. Dergachev, A Novel Universal Statistic for Computing Upper Limits in Ill-behaved Background, *Phys. Rev. D* **87**, 062001 (2013).
- [31] C. Palomba *et al.*, Direct constraints on ultra-light boson mass from searches for continuous gravitational waves, *Phys. Rev. Lett.* **123**, 171101 (2019)
- [32] B. P. Abbott *et al.* (LIGO Scientific Collaboration and Virgo Collaboration), All-sky Search for Periodic Gravitational Waves in the O1 LIGO Data, *Phys. Rev. D* **96**, 062002 (2017)
- [33] See EPAPS Document No. [number will be inserted by publisher] for numerical values of upper limits, outlier tables and hardware injection parameters. Also at <https://www.aei.mpg.de/continuouswaves/02Falcon500-1700>
- [34] A. Arvanitaki, M. Baryakhtar, and X. Huang, Discovering the QCD axion with black holes and gravitational waves, *Phys. Rev. D* **91**, 084011 (2015)
- [35] S. J. Zhu, M. Baryakhtar, M. A. Papa, D. Tsuna,

- N. Kawanaka and H. Eggenstein, Characterizing the continuous gravitational-wave signal from boson clouds around Galactic isolated black holes, [arXiv:2003.03359 [gr-qc]].
- [36] O2 continuous hardware injection signal parameters https://www.gw-openscience.org/O2_injection_params
- [37] B. P. Abbott *et al.* [LIGO Scientific and Virgo], Observation of Gravitational Waves from a Binary Black Hole Merger, *Phys. Rev. Lett.* **116** (2016) no.6, 061102
- [38] C. Cutler and B. F. Schutz, The Generalized F-statistic: Multiple detectors and multiple GW pulsars, *Phys. Rev. D* **72** (2005), 063006